Upconversion luminescence of Er^{3+} in transparent SiO_2–PbF_2–ErF_3 glass ceramics

Y. KAWAMOTO*, R. KANNO, J. QIU
Division of Science of Materials, Graduate School of Science and Technology, Kobe University, Nada, Kobe 657, Japan

Oxyfluoride glasses with the composition $50SiO_2 \cdot 50PbF_2 \cdot xErF_3$ ($x = 4$ and 5) by molar ratio were developed. Transparent glass ceramics were obtained by heat-treating the $50SiO_2 \cdot 50PbF_2 \cdot xErF_3$ glasses at the first crystallization temperatures. X-ray diffraction analysis of the transparent glass ceramics revealed that fluorite type β-$PbF_2:Er^{3+}$ solid solution regions of about 13.0 nm in diameter are precipitated in the glass matrix. The formation of this β-$PbF_2:Er^{3+}$ solid solution was also supported by Eu^{3+} fluorescence spectra which were measured on specimens in which Eu substituted for Er. Under 800 nm laser excitation, the Er^{3+} upconversion luminescence of $50SiO_2 \cdot 50PbF_2 \cdot xErF_3$ glasses was barely detectable, but the $50SiO_2 \cdot 50PbF_2 \cdot xErF_3$ glass ceramics gave Er^{3+} upconversion luminescence at a very high efficiency. The reason for the highly efficient Er^{3+} upconversion luminescence in the $50SiO_2 \cdot 50PbF_2 \cdot xErF_3$ glass ceramics can be explained in terms of the very small multiphonon relaxation rates that are anticipated from consideration of the Eu^{3+} emission spectra.

1. Introduction

To date, the upconversion luminescence characteristics of rare-earth ions such as Er^{3+}, Tm^{3+}, Ho^{3+} and Nd^{3+} have been studied in glass systems based on oxides [1], fluorides [2], chlorides [3], bromides [4], iodides [4] and sulfides [5]. When the practical utility of these glass systems is judged from the standpoint of chemical durability and processing oxide glass systems are considered to be the best host for rare-earth ions. Unfortunately however, non-radiative decay rates in oxide glasses are very large because of high phonon frequencies [6]. Thus, the efficiency of upconversion luminescence in oxide glasses is extremely low, compared with those in halide and sulfide glasses. Consequently oxide glasses in which upconversion luminescence can be observed are limited to germanate [7], tellurite [1] and gallate [1] glasses that have comparatively low phonon energies. Unfortunately silicate glasses, which are the most chemically and mechanically stable amongst the various oxide glass systems, have only very faint upconversion luminescence due to their large phonon energies [8].

Recently the present authors found that oxyfluoride glasses can be obtained in the SiO_2–PbF_2–ErF_3 system and that the heat treatment of the glasses gives transparent glass ceramics in which β-$PbF_2:Er^{3+}$ crystallites are dispersed in the glass matrix. This glass ceramics gave a highly efficient upconversion luminescence under 800 nm laser excitation.

This paper reports on the upconversion luminescence characteristics of Er^{3+} in the transparent SiO_2–PbF_2–ErF_3 glass ceramics.

2. Experimental procedure and results

2.1. Sample preparation

Oxyfluoride glasses with compositions of $50SiO_2 \cdot 50PbF_2 \cdot xErF_3$ ($x = 3$, 4 and 5) and $50SiO_2 \cdot 50PbF_2 \cdot 1EuF_3$ by molar ratio were prepared from high purity SiO_2, PbF_2, ErF_3 and EuF_3 reagents. The 5 g batches of the raw materials were melted at 1000 °C for 25 min in covered Pt crucibles in the atmosphere. The melts were then pressed by two brass plates kept at 100–150 °C. The glasses obtained were annealed at the respective glass-transition temperatures that had been determined from differential thermal analysis (DTA) scans obtained with a Rigaku TAS100 differential thermal analyser.

Fig. 1 shows the DTA curves of the $50SiO_2 \cdot 50PbF_2 \cdot xErF_3$ glasses where T_g and T_x indicate the glass transition temperatures and the first crystallization temperatures, respectively.

2.2. Heat treatment of the glasses

The $50SiO_2 \cdot 50PbF_2 \cdot xErF_3$ ($x = 3$, 4 and 5) and $50SiO_2 \cdot 50PbF_2 \cdot 1EuF_3$ glasses were heat-treated at the first crystallization temperature *in vacuo*. After the heat treatment, X-ray diffraction (XRD) measurements

* Corresponding author

0022–2461

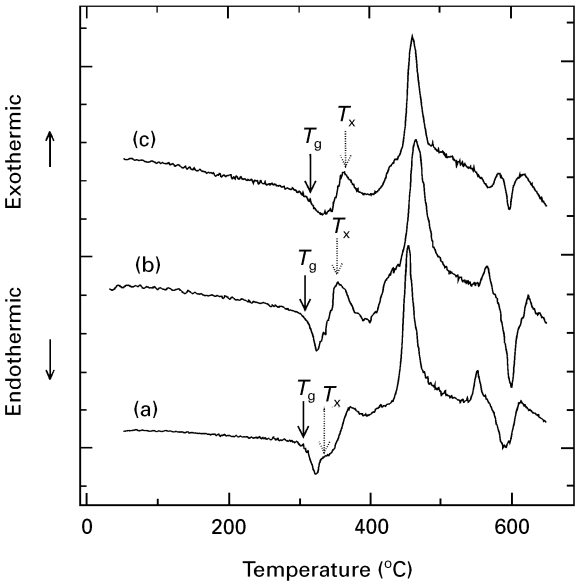

Figure 1 DTA curves of the glass of compositions $50SiO_2 \cdot 50PbF_2 \cdot xErF_3$ with x equal to: (a) 3; (b) 4 and (c) 5.

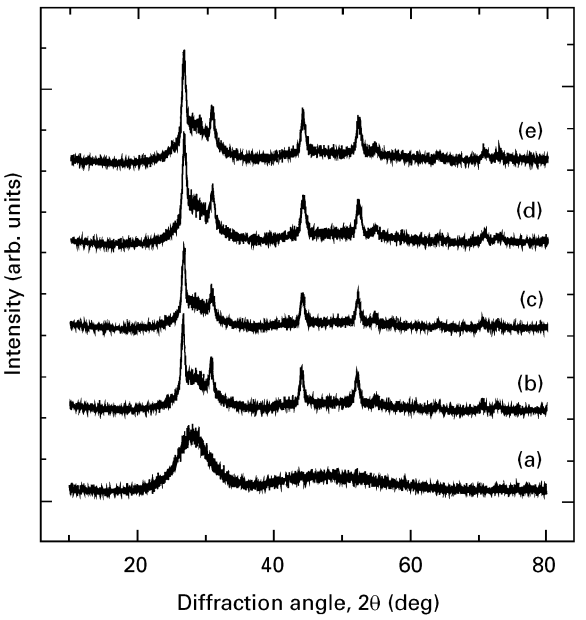

Figure 2 The XRD patterns of $50SiO_2 \cdot 50PbF_2 \cdot 5ErF_3$ glass heat-treated at the first crystallization temperature for (a) 0 h, (b) 0.5 h, (c) 1 h, (d) 3 h and (e) 6 h.

were carried out using a Rigaku RAD-C System X-ray diffractometer that produced CuK_α radiation.

Fig. 2 shows the XRD patterns of the $50SiO_2 \cdot 50PbF_2 \cdot 5ErF_3$ glass heat-treated at the first glass transition temperature for 0, 0.5, 1, 3 and 6 h. The XRD patterns of heat-treated glasses indicate that crystalline materials are precipitated in the glass matrices. The heat treatment of the $50SiO_2 \cdot 50PbF_2 \cdot 3ErF_3$, $50SiO_2 \cdot 50PbF_2 \cdot 4ErF_3$ and $50SiO_2 \cdot 50PbF_2 \cdot 1EuF_3$ glasses also gave the same XRD patterns. Despite the precipitation of crystalline materials, the heat-treated $50SiO_2 \cdot 50PbF_2 \cdot 4ErF_3$ and $50SiO_2 \cdot 50PbF_2 \cdot 5ErF_3$ glasses showed no changes in transparency. However on the other hand, the $50SiO_2 \cdot 50PbF_2 \cdot 3ErF_3$ glass became slightly translucent under the heat treatment. Thus, the $50SiO_2 \cdot 50PbF_2 \cdot 3ErF_3$ glass was omitted from the present experiments.

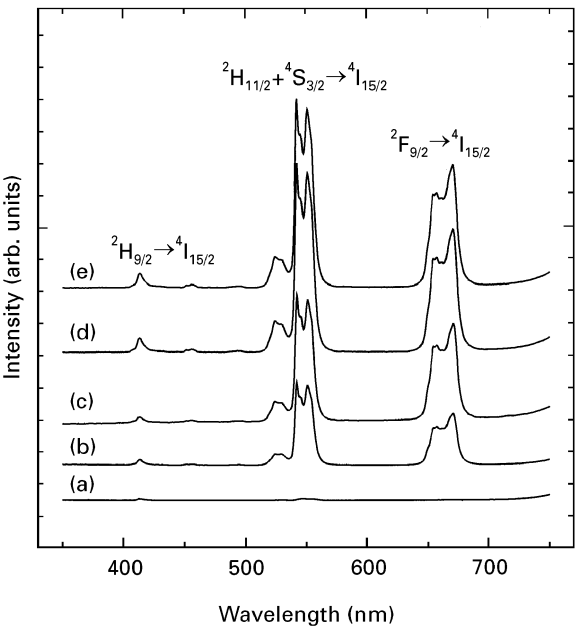

Figure 3 The upconversion luminescence spectra of Er^{3+} in the $50SiO_2 \cdot 50PbF_2 \cdot 5ErF_3$ glass heat-treated at the first crystallization temperature for: (a) 0 h, (b) 0.5 h, (c) 1 h, (d) 3 h and (e) 6 h.

2.3. Upconversion luminescence spectra of Er^{3+}

The Er^{3+} upconversion luminescence spectra of the $50SiO_2 \cdot 50PbF_2 \cdot xErF_3$ ($x = 4$ and 5) glasses and glass ceramics were measured over the wavelength range of 350–750 nm with an Hitachi F-3010 fluorescence spectrophotometer at ambient temperature, using 800 nm radiation from an AlGaAs diode laser (Sony, SLD303XT-22) with a 325 mW power. Specimens with a size of $5.0 \times 6.0 \times 1.2$ mm with optically flat surfaces were used in the measurements.

Fig. 3 shows the change in the upconversion luminescence spectra with heat treatment time for the $50SiO_2 \cdot 50PbF_2 \cdot 5ErF_3$ composition. The $50SiO_2 \cdot 50PbF_2 \cdot 4ErF_3$ composition also showed almost the same spectral change with heat-treatment time.

2.4. Emission and excitation spectra of Eu^{3+}

The emission spectra of the $^5D_0 \rightarrow {}^7F_J$ ($J = 0$, 1 and 2) transitions of Eu^{3+} in the $50SiO_2 \cdot 50PbF_2 \cdot 1EuF_3$ glass and glass ceramics were measured over the wavelength range of 570–650 nm with a Hitachi F3010 fluorescence spectrophotometer at room temperature, using the 395 nm light of a Xe lamp as the excitation source. Fig. 4 shows the change in the Eu^{3+} emission spectra with heat-treatment time for the $50SiO_2 \cdot 50PbF_2 \cdot 1EuF_3$ composition.

The excitation spectra of Eu^{3+} in the $50SiO_2 \cdot 50PbF_2 \cdot 1EuF_3$ glass and glass ceramics sample were measured by monitoring the $^5D_0 \rightarrow {}^7F_2$ emission at 616 nm. The measurement was performed over the wavelength range of 420–475 nm at room temperature with the same apparatus as that used for the emission measurements. Fig. 5 shows the change in Eu^{3+} excitation spectra with heat-treatment time for the $50SiO_2 \cdot 50PbF_2 \cdot 1EuF_3$ composition.

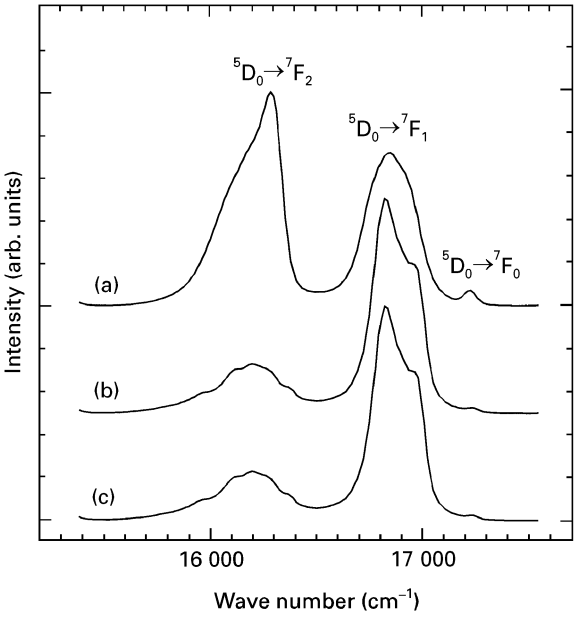

Figure 4 The Eu^{3+} emission spectra of the $50SiO_2 \cdot 50PbF_2 \cdot 1EuF_3$ glass heat-treated at the first crystallization temperature for: (a) 0 h, (b) 0.5 h and (c) 3 h.

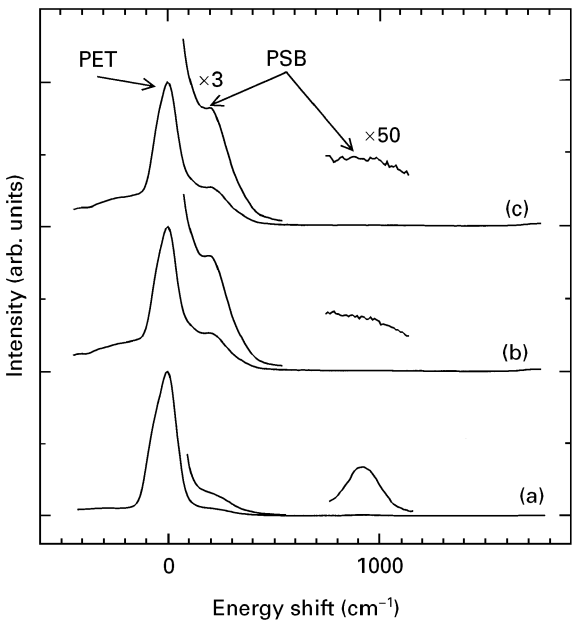

Figure 5 The Eu^{3+} excitation spectra of the $50SiO_2 \cdot 50PbF_2 \cdot 1EuF_3$ glass heat-treated at the first crystallization temperature for (a) 0 h, (b) 0.5 h and (c) 3 h.

2.5. Raman scattering spectrum

The Raman scattering spectrum of a β-PbF_2 crystal (a polycrystalline disc) were measured over the wave number range of 50–1200 cm^{-1} with a Perkin Elmer Spectrum 2000R FT-Raman spectrometer at ambient temperature. Fig. 6 shows the Raman scattering spectrum of the β-PbF_2 crystal.

3. Discussion

The crystallization behaviour of the $50SiO_2 \cdot 50PbF_2 \cdot xErF_3$ ($x = 4$ and 5) glasses is discussed first. As mentioned in Section 2.2, the XRD patterns of the

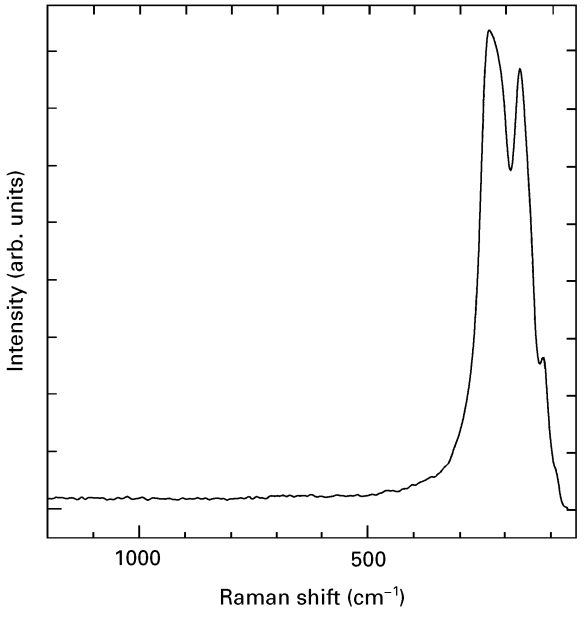

Figure 6 The Raman scattering spectrum of the β-PbF_2 crystal.

crystalline precipitate are entirely the same regardless of the glass composition and heat treatment time.

Fig. 7 shows a comparison of the XRD pattern of the crystalline precipitate with that of the β-PbF_2 crystal. The use of the Debye–Scherrer equation enabled the size of the crystalline precipitate to be evaluated as approximately 13.0 nm in diameter. The diffraction peaks of the crystalline precipitate can be indexed in terms of the fluorite structure (space group: Fm3m) with a lattice constant $a = 0.582$ nm whose Miller indices are given in Fig. 7. The lattice constant of the β-PbF_2 crystal in the fluorite structure is $a = 0.5940$ nm [9]. The slightly small lattice constant of the present crystalline precipitate indicates that it is a solid solution of the type β-PbF_2:Er^{3+} in which Pb^{2+} ions with an ionic radius of 0.129 nm are partially substituted by Er^{3+} ions with an ionic radius of 0.100 nm. This interpretation is supported by the Eu^{3+} emission spectra of the $50SiO_2 \cdot 50PbF_2 \cdot 1EuF_3$ glass and glass ceramic, as will be discussed below.

In the emission bands of Eu^{3+} (see Fig. 4), the $^5D_0 \rightarrow {}^7F_2$ emission band is due to the electric-dipole transition, which largely depends on the local symmetry of the co-ordination environment around Eu^{3+}, while the $^5D_0 \rightarrow {}^7F_1$ emission band is due to the magnetic-dipole transition, which is independent of the local symmetry. Therefore, the ratio of the $^5D_0 \rightarrow {}^7F_2$ to $^5D_0 \rightarrow {}^7F_1$ emission intensities gives information about the deviation from inversion symmetry in the co-ordination environment of the Eu^{3+}. Fig. 8 shows the ratios of the $^5D_0 \rightarrow {}^7F_2$ to $^5D_0 \rightarrow {}^7F_1$ emission intensities in the $50SiO_2 \cdot 50PbF_2 \cdot 1EuF_3$ glass and the $50SiO_2 \cdot 50PbF_2 \cdot 1EuF_3$ glass ceramics. From this figure, it can be seen that the ratio varies from about 1.6 for the glass to about 0.3 for the glass ceramics. A pronounced decrease in the ratio implies that in the crystallization process Eu^{3+} ions in the glass are incorporated into the β-PbF_2 crystallites, leading to a high symmetry in the co-ordination environment around Eu^{3+}.

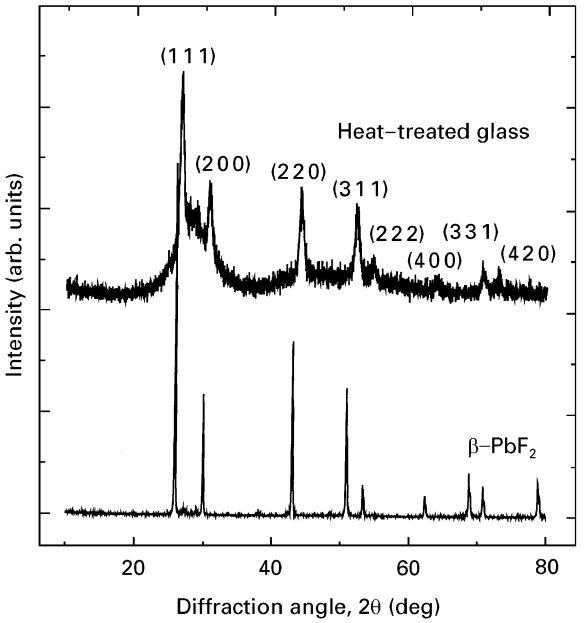

Figure 7 A comparison of the XRD pattern of the crystalline precipitate with that of the β-PbF_2 crystal.

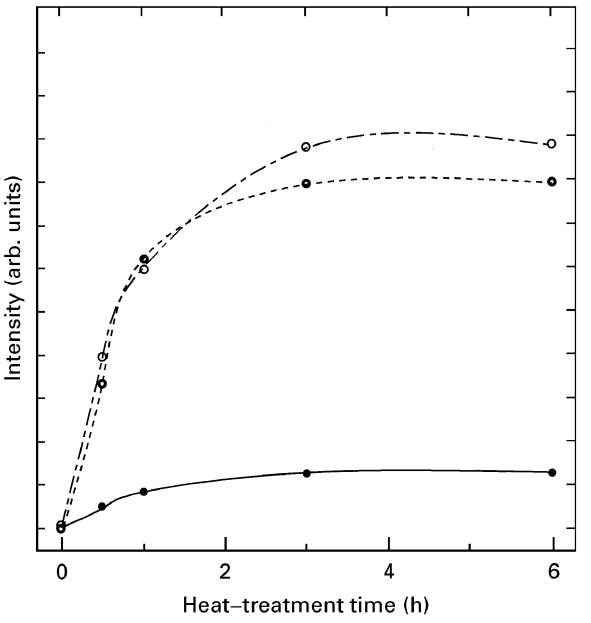

Figure 9 The relationship between the upconversion luminescence intensity and heat treatment time for the $50SiO_2 \cdot 50PbF_2 \cdot 5ErF_3$ composition. Key: (●) $^2H_{11/2} \rightarrow {}^4I_{15/2}$, (○) $^4S_{3/2} \rightarrow {}^4I_{15/2}$ and (●) $^4F_{9/2} \rightarrow {}^4I_{15/2}$.

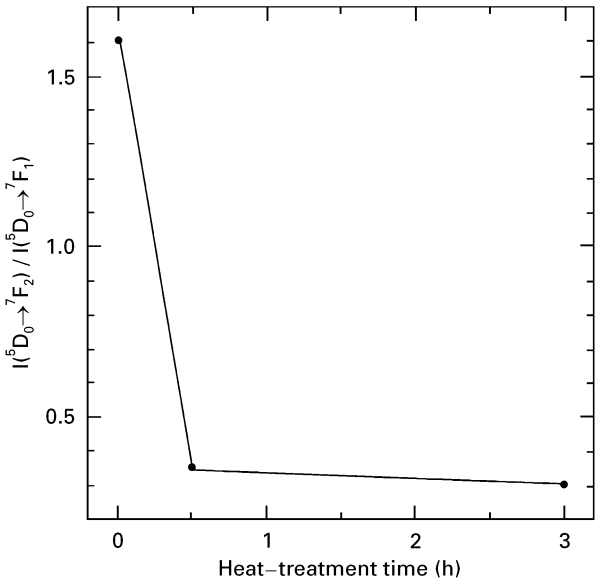

Figure 8 The ratio of the $^5D_0 \rightarrow 7F_2$ to $^5D_0 \rightarrow {}^7F_1$ emission intensities for the $50SiO_2 \cdot 50PbF_2 \cdot 1EuF_3$ glass and $50SiO_2 \cdot 50PbF_2 \cdot 1EuF_3$ glass ceramics.

Next, the Er^{3+} upconversion luminescence characteristics of the $50SiO_2 \cdot 50PbF_2 \cdot xErF_3$ ($x = 4$ and 5) glasses and glass ceramic samples are discussed. As is shown in Fig. 3, the Er^{3+} upconversion luminescence of the $50SiO_2 \cdot 50PbF_2 \cdot xErF_3$ glasses is hardly detectable, but the $50SiO_2 \cdot 50PbF_2 \cdot xErF_3$ glass ceramics show Er^{3+} upconversion luminescence at a very high efficiency. Furthermore, the upconversion luminescence intensity of the glass ceramics increases with heat treatment time, becoming saturated around a heat-treatment time of 3 h. The relationship between the intensity of the upconversion luminescence and the heat treatment time, observed for the $50SiO_2 \cdot 50PbF_2 \cdot 5ErF_3$ composition, is shown in Fig. 9. Almost the same relationship was observed for the $50SiO_2 \cdot 50PbF_2 \cdot 4ErF_3$ composition.

According to the Miyakawa–Dexter equation [6], the nonradiative decay rate due to a multiphonon relaxation process is governed by the phonon energy and the electron–phonon coupling strength. The larger the phonon energy and/or the electron–phonon coupling strength, the larger the decay rate. That is to say, a decrease in the phonon energy and/or electron–phonon coupling strength increases the lifetime and quantum efficiency of excited levels, and consequently increases the emission intensity of the upconversion luminescence.

The phonon sideband (PSB) spectra of the $50SiO_2 \cdot 50PbF_2 \cdot 1EuF_3$ glass and glass ceramics have already been shown in Fig. 5. In the figure all the spectra are normalized to the intensity of the pure electronic transition (PET) in order to facilitate a comparison of the spectra. The phonon energy corresponds to the mean energy difference between the PET and the PSB, and the electron–phonon coupling strength is estimated as the ratio of the integrated intensity of the PSB to that of the PET.

In order to evaluate both the phonon frequency and electron–phonon coupling strength from Fig. 5, the deconvolution of the phonon sidebands from the pure electronic transition bands was carried out using a curve-fitting program that applied the least squares method. The result obtained for the $50SiO_2 \cdot 50PbF_2 \cdot 1EuF_3$ composition is shown in Fig. 10 (a and b) which reveals that phonon frequencies are observed around 200 and 930 cm^{-1}, and that the electron–phonon coupling strength at 200 cm^{-1} is small for the glass and large for the glass ceramics, while that at 930 cm^{-1} is large for the glass and small for the glass ceramics. These results imply that

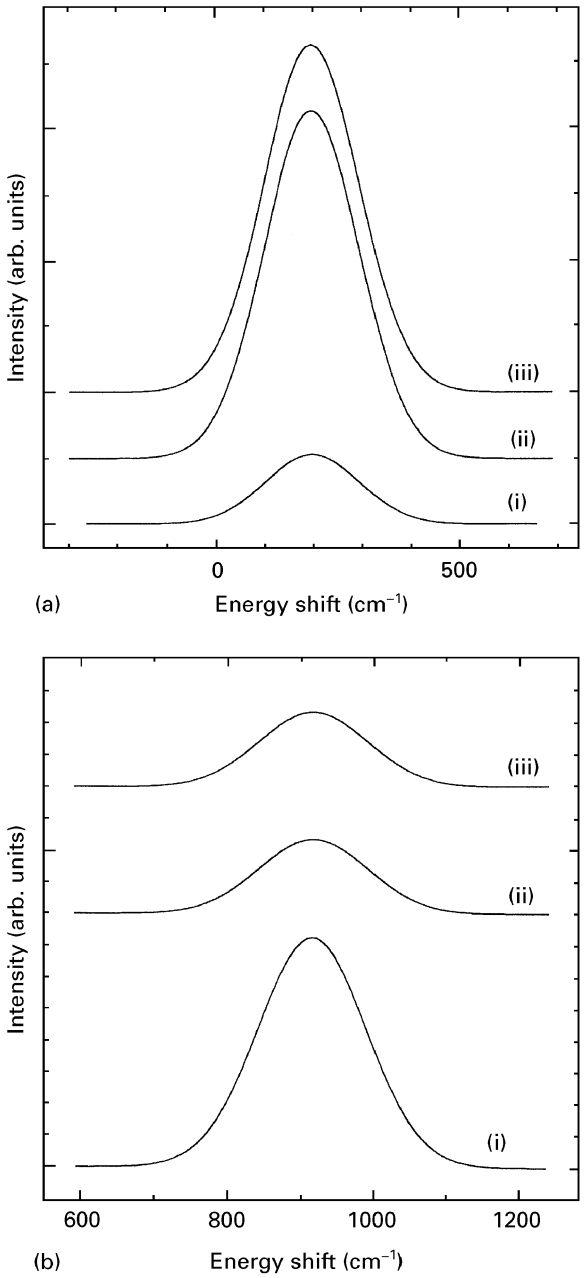

Figure 10 Extracted phonon sidebands of (a) $50SiO_2 \cdot 50PbF_2 \cdot 1EuF_3$ glass at heat treatment times of (i) 0 h, (ii) 0.5 h and (iii) 3 h and (b) $50SiO_2 \cdot 50PbF_2 \cdot 1EuF_3$ glass heat treated for (i) 0 h, (ii) 0.5 h and (iii) 3 h.

the Er^{3+} ions in the glass are strongly coupled to the phonon mode at 930 cm^{-1}, causing an increase in the non-radiative decay rate due to multiphonon relaxation. On the other hand, the Er^{3+} ions in the glass ceramics are strongly coupled to the phonon mode at 200 cm^{-1}, which leads to a decrease in the non-radiative decay rate. This is the reason why the Er^{3+} upconversion luminescence is barely observed for the $50SiO_2 \cdot 50PbF_2 \cdot xErF_3$ glass, but it is strongly observed for the $50SiO_2 \cdot 50PbF_2 \cdot xErF_3$ glass ceramics.

Finally the assignment of the phonon modes at 200 and 930 cm^{-1} is discussed. A phonon mode at about 200 cm^{-1} can be assigned to a lattice vibration of the β-PbF_2 crystal, since β-PbF_2 gives a Raman peak around 200 cm^{-1} (see Fig. 6). On the other hand, the phonon mode at about 930 cm^{-1} may be assigned to a symmetric stretching vibration of a SiO_4 tetrahedra with two non-bridging oxygens and two bridging oxygens and/or that of a SiO_4 tetrahedron with three non-bridging oxygens and one bridging oxygen [10].

We note that Wang and Ohwaki have developed a transparent oxyfluoride glass ceramic with a composition of $15SiO_2 \cdot 15AlO_{1.5} \cdot 24PbF_2 \cdot 20CdF_2 \cdot 10YbF_3 \cdot 1ErF_3$ (composition in mol%) and have observed highly efficient upconversion luminescence under 0.97 μm laser excitation [11].

4. Conclusion

Glasses have been developed in the SiO_2–PbF_2–ErF_3 system. The heat treatment of the $50SiO_2 \cdot 50PbF_2 \cdot 5ErF_3$ and $50SiO_2 \cdot 50PbF_2 \cdot 4ErF_3$ glasses at the first glass transition temperatures gave transparent glass ceramics in which β-PbF_2:Er^{3+} crystallites with a diameter of about 13.0 nm are dispersed in the glass matrix. Little upconversion luminescence from Er^{3+} was observed for the $50SiO_2 \cdot 50PbF_2 \cdot 5ErF_3$ and $50SiO_2 \cdot 50PbF_2 \cdot 4ErF_3$ glasses. However, the $50SiO_2 \cdot 50PbF_2 \cdot 5ErF_3$ and $50SiO_2 \cdot 50PbF_2 \cdot 4ErF_3$ glass ceramics showed upconversion luminescence with a high efficiency. This phenomenon is due to a difference in the phonon mode that is coupled to the Er^{3+} ions in the glass and glass ceramics. The Er^{3+} ions in the glass are strongly coupled to a phonon mode at approximately 930 cm^{-1}, while Er^{3+} ions in the glass ceramics are strongly coupled to the phonon mode at approximately 200 cm^{-1}. Therefore, the multiphonon relaxation rate in the glass ceramics is very small as compared with that in the glass. This leads to highly efficient upconversion luminescence behaviour for the glass ceramics. The difference in the phonon mode between the glass and glass ceramic is due to a difference in the co-ordination environment around the Er^{3+} ions.

References

1. S. TANABE, K. HIRAO and N. SOGA, *J. Non-Cryst. Solids* **122** (1990) 79.
2. S. TANABE, K. TAKAHARA, M. TAKAHASHI and Y. KAWAMOTO, *J. Opt. Soc. Amer. B* **12** (1995) 786.
3. M. SHOJIYA, M. TAKAHASHI, R. KANNO, Y. KAWAMOTO and K. KADONO, *Appl. Phys. Lett.* **65** (1994) 1874.
4. *Idem*, *ibid* **67** (1995) 2453.
5. K. KADONO, H. HIGUCHI, M. TAKAHASHI, Y. KAWAMOTO and H. TANAKA, *J. Non-Cryst. Solids* **184** (1995) 309.
6. T. MIYAKAWA and D. L. DEXTER, *Phys. Rev. B* **1** (1970) 2961.
7. Z. PAN, S. H. MORGAN, K. DYER, A. UEDA and H. LIU, *J. Appl. Phys.* **79** (1996) 8906.
8. R. S. QUIMBY, M. G. DREXHAGE and M. J. SUSCAVAGE, *Electron. Lett.* **23** (1987) 32.
9. JCPDS International Centre for Diffraction Data Card no. 6-0251.
10. P. McMILLAN, *Amer. Mineralogist* **69** (1984) 622.
11. Y. WANG and J. OHWAKI, *Appl. Phys. Lett.* **63** (1993) 3268.

Received 31 October 1996
and accepted 18 July 1997